European Journal of Radiology 112 (2019) 180–185

Contents lists available at ScienceDirect

European Journal of Radiology

journal homepage: www.elsevier.com/locate/ejrad

Research article

Separation between the chest wall and subpleural lung lesions: A two-step method to preoperatively exclude invasion or focal pleural adhesion by multidetector computed tomography

Mitsuko Tsubamoto[a,*], Takahiro Nishida[a], Naozumi Higaki[b], Seiji Taniguchi[b], Tatsuhito Takeshima[a], Yuichi Sasaki[a], Takumi Kataoka[a], Kenji Nishibayashi[a], Toshiyuki Ikeda[c]

[a] Department of Radiology, Nishinomiya Municipal Central Hospital, 8-24, Hayashida-cho, Nishinomiya-city, Hyogo, 663-8014, Japan
[b] Department of Thoracic Surgery, Nishinomiya Municipal Central Hospital, 8-24, Hayashida-cho, Nishinomiya-city, Hyogo, 663-8014, Japan
[c] Department of Respiratory Medicine, Nishinomiya Municipal Central Hospital, 8-24, Hayashida-cho, Nishinomiya-city, Hyogo, 663-8014, Japan

ARTICLE INFO

Keywords:
Computed tomography
Parietal pleural invasion
Non-small cell lung cancer
Inspiratory phase
Expiratory phase
Affected-side-up lateral decubitus position

ABSTRACT

Purpose: To develop and assess a non-invasive two-step method for evaluating the relationship between the parietal pleura and peripheral pulmonary lesions to preoperatively exclude invasion or focal pleural adhesion by multidetector computed tomography (CT).

Methods: Twenty-six patients with pulmonary peripheral lesions who underwent surgical lung resection between May and December 2017 were enrolled in this study. Routine CT was performed in the inspiratory phase in the supine position. Additional CT examinations were performed both in inspiratory and expiratory phases in the affected-side-up lateral position. Axial, sagittal, and coronal images were reconstructed from the CT data. In the first-step analysis, we evaluated the separation between the chest wall and subpleural lung lesions (separation) by comparing inspiratory- and expiratory-phase images obtained in the affected-side-up lateral position. When the separation was absent, we performed a second-step analysis, where we compared images obtained in the supine position during routine CT with those obtained in the affected-side-up lateral position and subsequently assessed the presence and absence of the separation.

Results: In the first-step analysis, the separation was observed in 21 lesions, which were categorised as showing "no invasion" or "no focal adhesion" on the basis of histological findings. After the second-step analysis, the separation was absent in three lesions and present in two; the latter two lesions were categorised as showing "no invasion" or "no focal adhesion" on the basis of operative and histological findings. Of the three lesions that did not exhibit the separation in either step of the analysis, two were diagnosed as exhibiting parietal pleural invasion on the basis of histological findings, while the third was categorised as showing "no invasion" or "no focal adhesion" on the basis of operative and histological findings. The sensitivity, specificity, positive and negative predictive values, and accuracy of this two-step method were 96% (95% confidence interval [CI]: 79–100%), 100% (95% CI: 16–100%), 100%, 67% (95% CI: 23–93%), and 96% (95% CI: 80–100%), respectively.

Conclusions: Our two-step method is especially useful for excluding the parietal pleural involvement of peripheral pulmonary lesions. Even when the separation between the chest wall and subpleural lung lesions was limited, the change in position was useful for observing the separation and excluding parietal pleural involvement. This novel two-step method also has the advantage of being simple, cost-effective, and universally available.

Abbreviations: 2D, two-dimensional; 3D, three-dimensional; 4D, four-dimensional; ad., adenocarcinoma; AUC, area under the ROC curve; CI, confidence interval; CT, computed tomography; DS, distance of separation; LUL, left upper lobe; MRI, magnetic resonance imaging; RLL, right lower lobe; ROC, receiver operating characteristic; RUL, right upper lobe; sq, squamous cell carcinoma

* Corresponding author.
E-mail addresses: mikko@mud.biglobe.ne.jp (M. Tsubamoto), nisshi56@nishi.or.jp (T. Nishida), naohigaki@aol.com (N. Higaki), hijiriosamu@yahoo.co.jp (S. Taniguchi), takashimatatsu@yahoo.co.jp (T. Takeshima), yuichi890409@yahoo.co.jp (Y. Sasaki), tkm.k0593@hotmail.co.jp (T. Kataoka), makoriku1965@yahoo.co.jp (K. Nishibayashi), med22@nishi-hp.jp (T. Ikeda).

https://doi.org/10.1016/j.ejrad.2019.01.027
Received 2 June 2018; Received in revised form 21 December 2018; Accepted 24 January 2019

1. Introduction

Many imaging modalities, including computed tomography (CT), magnetic resonance imaging (MRI), and positron emission tomography with 2-deoxy-2-fluoro-D-glucose, are often used for staging lung cancer, estimating cranial metastasis, and evaluating lymphatic and distant metastases. However, CT is the most reliable imaging modality for assessment of local invasion of peripheral lung cancer in typical clinical settings. The presence or absence of parietal pleural invasion not only alters the T-stage classification of a tumour but also influences surgical planning; en block resection is recommended for pl3 (pleural invasion into any component of the parietal pleura or chest wall) lung cancer involving the chest wall [1–4]. Therefore, accurate estimation of the relationship between the parietal pleura and subpleural lung lesions is essential before starting therapy.

Unfortunately, existing preoperative examinations cannot reveal whether or not a pleural invasion or adhesion is present unless the chest-wall invasion is obvious. Although many investigators have reported on the preoperative evaluation of parietal pleural invasion of peripheral lung cancer [5–15], it has remained an unsolved challenge for a long time. Static CT images have been employed for evaluation of parietal pleural invasion [11,12]. Ebara et al. morphologically evaluated static images of peripheral lung tumours, including those measuring ≤ 3 cm in diameter, using a computer analysis application. Although the authors attempted to determine both parietal and visceral pleural invasion, the accuracy of detection of parietal pleural invasion was limited [11]. Imai et al. reported that the ratio of the interface length between the tumour and the structure adjacent to the maximum tumour diameter provides a high accuracy for predicting parietal pleural invasion [12]. Although these authors used a simple and non-invasive method, they only evaluated tumours that were > 3 cm in diameter, because their method could not be applied to smaller tumours.

Since the advent of area-detector CT, several authors have reported new evaluation criteria using dynamic-ventilatory scanning with quantitative four-dimensional (4D) CT [16,17]. Although this method is promising, it requires the latest technology and is not available at all institutions that have CT machines.

The purpose of our study was to develop and assess a non-invasive preoperative method, termed the two-step method, for evaluating the relationship between the parietal pleura and peripheral pulmonary lesions in order to preoperatively exclude invasion or focal pleural adhesion by multidetector CT.

2. Material and methods

The institutional review board approved this prospective study, and all patients provided informed consent.

2.1. Subjects

Twenty-six patients with a peripheral pulmonary lesion abutting the chest wall or a pleural indentation before surgery were included in this study between May and December 2017. Pulmonary lesions abutting the mediastinum and interlobar pleura were excluded because we were unable to set the anatomical index to calculate the distance of movement or superimpose the structure to assess the separation between the chest wall and subpleural lung lesions.

This study included 11 women and 15 men (median age, 69 years; range, 42–80 years) and 26 lesions (Table 1). The pulmonary lesions were located in the right upper lobe (n = 11), right middle lobe (n = 1), right lower lobe (n = 4), left upper lobe (n = 6), and lower lobe (n = 4). The average value of the maximum lesion diameter on axial CT images was 31.03 mm (range, 6–100 mm). Histopathological findings revealed the lesions to correspond to adenocarcinoma (n = 15), squamous cell carcinoma (n = 6), pleomorphic carcinoma (n = 1), metastatic lung cancer from breast cancer (n = 1), aspergilloma in a pre-existing cavity (n = 1), *Mycobacterium avium* complex (n = 1), and nonspecific inflammatory lesion (n = 1).

Table 1
Demographic and clinical characteristics of patients enrolled in this study.

Variable	Datum
No. of patients	26
Men/women	15/11
Median age (years)	69 (range, 42–80)
Tumour location	
Right upper lobe	11
Right middle lobe	1
Right lower lobe	4
Left upper lobe	6
Left lower lobe	4
Average tumour size (mm)	31.03 (range, 6–100)
Histological diagnosis	
Adenocarcinoma	15
Squamous cell carcinoma	6
Pleomorphic	1
Others	4
Pleural status	
No focal adhesion	26
Pleural adhesion away from the pulmonary lesion	7
pl0	7
pl1	12
pl2	1
pl3	2

Note — Except where otherwise mentioned, the data indicate the number of patients. pl0, absence of pleural invasion beyond the elastic layer; pl1, pleural invasion beyond the elastic layer; pl2, pleural invasion to the pleural surface; pl3, invasion into any component of the parietal pleura.

2.2. CT procedure

A 64-row-detector CT scanner (SOMATOM definition AS +; Siemens Healthineers, Erlangen, Germany) was used for CT examination. For scanning, the tube voltage was set at 100 or 120 kVp, and tube current was applied at auto milliampere settings in accordance with the CARE Dose 4D system for exposure-dose reduction. A first routine preoperative CT examination in the inspiratory phase was performed in the supine position with or without contrast media. Following this, a second scan was obtained with the patients positioned with their affected side up. Before image acquisition, the patients were given breathing instructions by the technologists. They taught the patients to inspire and expire as deeply as possible with costal breathing. The second CT image, including the lesion and the first or twelfth thoracic vertebra, was acquired in the full inspiratory and expiratory phases in the affected-side-up lateral decubitus position. Using the data acquired in the supine position as well as in the full inspiratory and expiratory phases in the affected-side-up lateral decubitus position, high-resolution axial CT images were reconstructed with a thickness of 2.0 mm. Sagittal and coronal images were also reconstructed with a thickness of 1.0 mm. A single image that included the longest interface abutting the chest wall or the point where the pleural tag attached to the chest wall was chosen from axial, sagittal, and coronal images in both the inspiratory and expiratory series. A chest-wall structure (e.g. the spine or a rib) was set as an index, which was used as a reference for superimposing images over each other in a workstation (Synapse Vincent, Fujifilm, Tokyo, Japan; Fig. 1).

2.3. Image analyses

Image analysis was performed without any histological or surgical information, before the patients received surgical treatment. In the first-step analysis, the separation between the chest wall and subpleural lung lesions was visually evaluated using axial, sagittal, and coronal images.

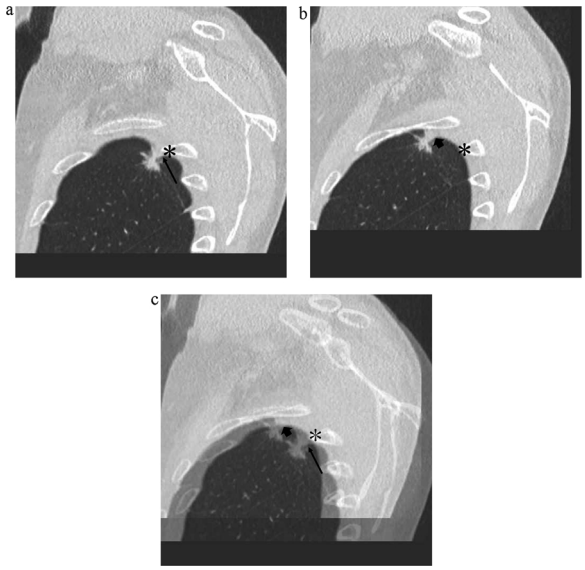

Fig. 1. A 58-year-old man with adenocarcinoma histologically diagnosed as pl1. Computed tomography images show a 17-mm nodule with pleural indentation in contact with the pleural surface. * Chest-wall index; →index on the peripheral lesion upon inspiration; ➧ index on the peripheral lesion upon expiration. (a) Sagittal image acquired in the lateral position upon inspiration. The distance between * and → is 6 mm. (b) Sagittal image acquired in the lateral position upon expiration. The distance between * and ➧ is 20.2 mm. (c) Superimposed image of (a) and (b) showing the separation between the chest wall and peripheral lesion. The distance of separation is 14.2 mm (20.2–6.0 mm). Note that the separation is also visually evident and easy to identify by visual analysis. One of the ribs (*) is set as an anatomical index for overlapping the two images.

Two observers manually, and in consensus, measured the distance between the peripheral lesions and the chest-wall index structure on axial, sagittal, and coronal images. When it was difficult to superimpose the chest-wall index structure, the separation was estimated by visual assessment. When the index on the chest wall was not included in the same plane as the subpleural lung lesion because of respiratory movement, the images were evaluated for any visually obvious separation; this meant that the distance of separation was too large to measure on a two-dimensional (2D) plane. When the index on the chest wall and the subpleural lung lesion were included in the same plane, the distance between the two was manually measured, and the difference between the inspiratory and expiratory phases was recorded as the distance of separation. The separation between the chest wall and subpleural lung lesions was considered to be present when the separation was visually obvious, or the distance of separation was more than 5 mm. In the absence of a separation in the first step analysis, the images were further evaluated by second-step analysis.

For the second-step analysis, routine inspiratory images acquired in the supine position were compared with inspiratory images obtained in the lateral position. The presence or absence of separation was evaluated in the same way as in the first-step analysis. The separation between the chest wall and subpleural lung lesions was considered to be present when the separation was visually obvious or the distance of separation was more than 5 mm.

2.4. Statistical analysis

Continuous variables were expressed as median/average and range. The sensitivity, specificity, positive and negative predictive values, and accuracy of the two-step method for estimating the absence of parietal pleural invasion or focal adhesion of subpleural lung lesions were determined.

The sample size was calculated on the basis of the assumption that this two-step method predicted no parietal pleural invasion or focal pleural adhesion, with an expected positive predictive value of 100%. The threshold value was 85%, which was based on the clinical utility.

For predicting the separation of pleura, receiver operating characteristic (ROC) curves were derived by plotting the relationship between specificity and sensitivity at various cut-off levels of distance. Obvious separation was defined as a distance of 43 mm, which was the maximum level of measurement. The accuracy of distance as a diagnostic tool for predicting separation observed during surgery was determined by calculating the area under the ROC curve (AUC), with AUC values > 0.90 indicating good accuracy. All statistical analyses were conducted using XLSTAT 2012 (Addinsoft, Paris, France).

3. Results

3.1. Assessment of radiation dose

For the additional CT images obtained in inspiratory and expiratory phases in the affected-side-up lateral position, the CT dose index volume was 4.5 ± 1.0 mGy (mean ± SD), and the dose–length product was 210.4 ± 67.3 mGycm. The total estimated radiation exposure for these additional CT images was 3.1 ± 1.0 mSv (using a conversion factor of 0.0145 for the chest) [18].

3.2. Two-step method

The ROC curve for predicting separation by means of distance had an AUC of 0.942 (95% confidential interval [CI], 0.866–1.000). Thus, distance was determined to be a good tool for predicting separation. At a threshold distance of 3.3 mm, the sensitivity, specificity, and positive and negative predictive values for predicting separation were 91.3%, 100%, 100%, and 60.0%, respectively; the corresponding values at a threshold distance of 5.9 mm were 87%, 100%, 100%, and 50.0%, respectively. Therefore, a distance of 5 mm was determined as a clinically convenient cut-off for predicting separation in this two-step method.

In the first-step analysis, the separation between the chest wall and subpleural lung lesions was present in 21 lesions. Among these, 13, 5, and 1 lesions on axial, sagittal, and coronal images, respectively, were considered as exhibiting obvious separation. All 21 lesions were categorised as showing “no invasion” or “no focal adhesion” on the basis of operative and histological findings (Figs. 1 and 2).

In the first-step analysis, the separation between the chest wall and subpleural lung lesions was absent in 5 of the 26 lesions. In the second-step analysis, the separation was considered to be absent in 3 and present in 2 of these 5 lesions. The latter two lesions were categorised as showing “no invasion” or “no focal adhesion” on the basis of operative and histological findings (Fig. 3). Of the three lesions that did not exhibit a separation between the chest wall and subpleural lung lesions in either step of the analysis, two were diagnosed as exhibiting parietal pleural invasion on the basis of histological findings (Fig. 4), while the third was categorised as showing “no invasion” or “no focal adhesion” on the basis of operative and histological findings. This false-positive lesion was located on the medial side of the right upper lobe (Table 2; Fig. 5).

The sensitivity, specificity, positive and negative predictive values, and accuracy of our two-step method for excluding parietal pleural invasion or focal adhesion of subpleural pulmonary lesions were 96% (23/24; 95% CI: 79–100%), 100% (2/2; 95% CI: 16–100%), 100% (23/23), 67% (2/3; 95% CI: 23–93%), and 96% (25/26; 95% CI: 80–100%), respectively. This study required 22 patients to achieve a one-sided significance level of 5% with a power of 80%. Factoring in a dropout rate of 4%, we set a target sample size of 23 patients with radiological diagnosis indicating no parietal pleural invasion or focal adhesion.

Pleural adhesion was observed in seven lesions during surgery. Because the sites of adhesion were all located away from the subpleural lung lesion of concern, they could not be reported in this study.

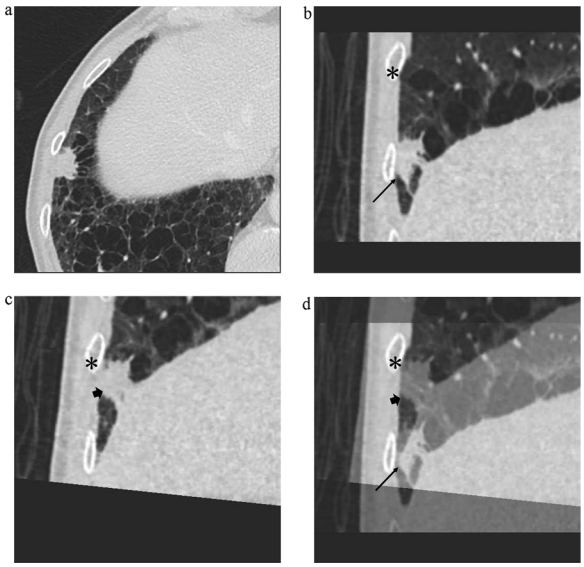

Fig. 2. A 76-year-old man with squamous cell carcinoma histologically diagnosed as pl1. Computed tomography (CT) images show a 17-mm nodule in contact with the pleural surface. * Chest-wall index; →index on the peripheral lesion upon inspiration; ➧ index on the peripheral lesion upon expiration. (a) High-resolution axial CT image acquired upon inspiration in the supine position during routine examination. It is difficult to make a reliable report about the invasion of the parietal pleura. (b) Coronal image acquired in the lateral position upon inspiration. The distance between * and → is 53.7 mm. (c) Coronal image acquired in the lateral position upon expiration. The distance between * and ➧ is 26 mm. (d) Superimposed image of (b) and (c) showing the separation. The distance of separation is 27.7 mm (53.7–26.0 mm). Note that the separation is also visually evident and easy to understand in the superimposed image.

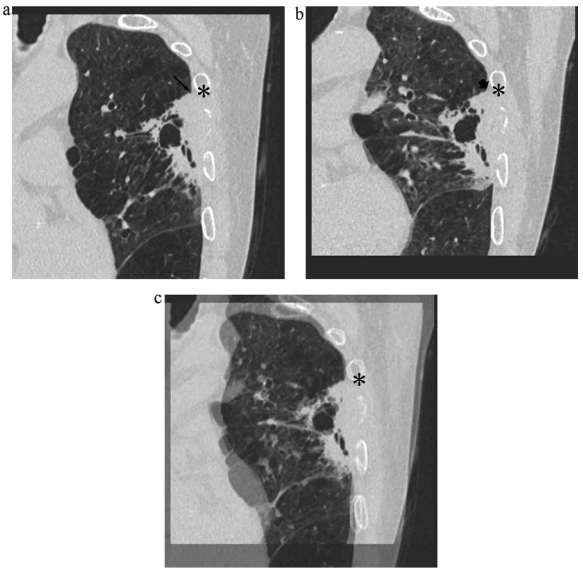

Fig. 4. A 75-year-old man with squamous cell carcinoma. After en bloc resection, the lesion was histologically diagnosed as pl3. Computed tomography images show a 42-mm cavitary nodule in contact with the chest wall; bone invasion is also observed. * Chest-wall index; →index on the peripheral lesion upon inspiration; ➧ index on the peripheral lesion upon expiration. (a) Coronal image acquired in the lateral position upon inspiration. The distance between * and → is 9.96 mm. (b) Coronal image acquired in the lateral position upon expiration. The distance between * and ➧ is 9.51 mm. (c) Superimposed image of (a) and (b). Note that the absence of separation is visually apparent. The distance of movement is 0.45 mm (9.96–9.51 mm).

Although video-assisted thoracoscopic surgery was changed to thoracotomy in a patient exhibiting a relatively broad and dense adhesion, the lesion had exhibited the separation in the first-step analysis.

4. Discussion

In compliance with a request from our surgeons, we attempted to develop a simple, non-invasive, preoperative method—termed the two-step method—for determining the relationship between the parietal pleura and subpleural lung lesions and for excluding parietal pleural involvement using a 64-row multidetector CT system.

Identifying an effective preoperative evaluation tool for pleural invasion of peripheral lung cancer has been an unsolved challenge for a long time. With regard to parietal pleural invasion, a previous study found that bony destruction with or without a soft-tissue mass extending into the chest wall was the only CT finding with a 100% positive predictive value for detection of parietal pleural and chest-wall invasion [15]. It has also been suggested that CT has limited accuracy for evaluating parietal pleural invasion when a tumour is abutting the pleura without bony destruction or a mass involving the chest wall [11].

We evaluated the separation between the chest wall and subpleural lung lesions by comparing images obtained in inspiratory and expiratory phases in the affected-side-up lateral decubitus position, which was similar to conducting a direct visual observation of respiratory movement. The separation between the chest wall and the subpleural lesions indicates that there is no fixation between the two structures, which implies the absence of parietal pleural invasion of subpleural lung cancer or pleural adhesion in that focal area. All patients in the present study were imaged by positioning the affected side up in the lateral decubitus position because it has been reported that, in the lateral position, the upper-lung capacity is greater than the lower-lung

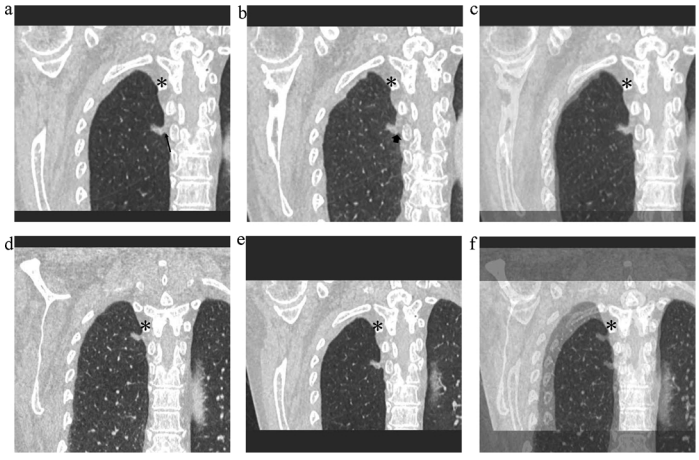

Fig. 3. A 76-year-old woman with adenocarcinoma histologically diagnosed as pl0. Computed tomography images show a 10-mm part-solid nodule with pleural indentation in contact with the pleural surface. * Chest-wall index; → index on the peripheral lesion upon inspiration; ➧ index on the peripheral lesion upon expiration. (a) Coronal image acquired in the lateral position upon inspiration. (b) Coronal image acquired in the lateral position upon expiration. (c) Superimposed image of (a) and (b). Note that the absence of separation is visually apparent. Our second-step analysis involved the following: (d) Reconstructed coronal image acquired in the supine position during routine examination; (e) coronal image acquired in the lateral position upon inspiration; and (f) superimposed image of (d) and (e). Note that the separation is present and quite obvious visually. Our second-step analysis is especially useful for estimating the region where the respiratory movement is small.

Table 2
Patients with no separation between the chest wall and subpleural lung lesions in the first-step analysis.

Patient no.	Age (years)	Sex	First-step analysis results	DS (mm/second-step)	Second-step analysis results	Pleural invasiveness	Location	Histological characteristics
1	75	M	Absent	2.5	Absent	pl3	LUL/S3 lateral	Sq.
2	76	F	Absent	Obvious	Present	pl0	RUL/S1 medial	Ad.
5	67	M	Absent	3.36	Absent	pl3	LUL/S1 + 2 lateral	Sq.
14	42	F	Absent	3.43	Absent	pl0	RUL/S1 medial	Ad.
20	80	F	Absent	Obvious	Present	pl1	RLL/S6 medial	Ad.

Note — These lesions were identified in the second-step analysis. Lesions exhibiting separation in the second-step analysis were categorised as showing "no pleural invasion" or "no focal adhesion" in accordance with operative and histological findings. The findings of the two steps of analysis were inconsistent only in one case (patient 14), where the lesion was located in the medial region of the right upper lobe. Ad., adenocarcinoma; DS, distance of separation; LUL, left upper lobe; pl0, absence of pleural invasion beyond the elastic layer; pl1, pleural invasion beyond the elastic layer; pl3, invasion into any component of the parietal pleura; RLL, right lower lobe; RUL, right upper lobe; Sq., squamous cell carcinoma.

capacity because of counteraction against the force of gravity [19].

In our study, when separation was observed in either the first- or second-step analysis, neither parietal pleural invasion nor focal adhesion was detected during surgery or histological examination. This two-step method for excluding parietal pleural involvement showed positive and negative predictive values of 100% and 67% (95% CI: 23–93%), respectively. Therefore, our two-step method is useful for ruling out parietal pleural involvement before surgery because it directly evaluates the separation between the chest wall and subpleural lesions.

In the first-step analysis, the separation was absent in case of three lesions with no histological findings of parietal pleural invasion. These three lesions were located in the medial and dorsal regions of the right upper lobe (two lesions) and in the superior segment of the right lower lobe (one lesion). Milic-Emili et al. reported that changes in lung volume during respiration are smaller in the upper-lung region than in the lower-lung region [20]. This might explain why the three lesions did not show the separation in the first-step analysis despite there being no evidence of parietal pleural invasion upon histological analysis — the lesions were located in a region that moves less during respiration. Moreover, these three lesions were located not only in the upper region but also in the medial and dorsal regions. To the best of our knowledge, this is a novel finding that the medial and dorsal regions of the upper-lung region exhibit only small changes in lung volume during respiration. However, the findings of the second-step analysis suggested another possibility. When routine images obtained in the inspiratory phase in the supine position were compared with images obtained in the affected-side-up lateral decubitus position, there were differences in the relationship between the chest-wall index structure and subpleural lesions in two of these three lesions, even though no separation was observed during respiration (in the first-step analysis). This finding suggests that change in body position reveals the separation, particularly in case of lesions located medial and dorsal to the upper lobe or in the superior segment of the lower lobe. Therefore, it is useful to perform the second-step analysis for lesions located in these regions. To the best of our knowledge, this finding is novel and has not been reported previously.

Recently, Choong et al. and Sakuma et al. investigated peripheral lung cancer invasion into adjacent structures using dynamic 4D CT. Sakuma et al. conducted quantitative analysis using an area-detector CT scanner and specialised software/workstations, making full use of the latest technology, and performed 3D and dynamic imaging, which allowed them to perform motion analysis for two adjacent structures [16,17]. Both studies reported that 4D CT is a useful and novel technology for conducting preoperative assessment of parietal pleural invasion/adhesion.

However, such latest technology is available at only a few institutions in the world. In contrast, our two-step method is simple and convenient and can be performed with most CT machines in the world. However, it is not applicable for evaluation of pleural adhesion that is located away from the peripheral pulmonary lesion. We strongly hope that dynamic 4D CT can play an important role in evaluation of pleural adhesion and provide more information about respiratory dynamics.

In the present study, we were unable to identify dense and broad adhesions preoperatively. This was because our two-step method was focused on evaluating the relationship between the parietal pleura and peripheral pulmonary nodules only focally; that is, our evaluation was focused only around the focal region of concern. We were, therefore, unable to identify dense adhesions located away from the region of

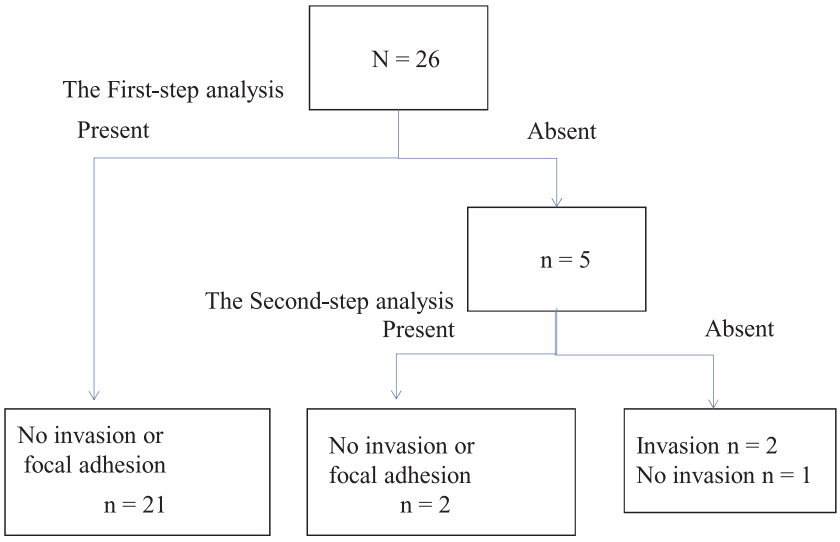

Fig. 5. Flowchart of the present study protocol. This two-step method for excluding parietal pleural involvement showed positive and negative predictive values of 100% and 67% (95% confidence interval: 23–93%), respectively. While the first-step analysis was based on respiratory movement, the second-step analysis was based on change in position.

concern, even when the distance was small.

There are several limitations to this study. Firstly, it included only a small number of patients. Patients with lesions abutting the great vessel, mediastinum, or interlobar fissure were not included. This was because we used a rib or the spine as an index for assessing the separation, and it would have been difficult to fix an index in the mediastinum or on an interlobar fissure. Secondly, we did not encounter any patients with focal pleural adhesion at the subpleural lung lesion. In case of patients with inflammatory diseases, although we suspected the presence of focal adhesion, it was non-existent. If a loose adhesion had existed, we might have observed the separation between the chest wall and subpleural lesions. We could not identify dense pleural adhesions that were located a little away from the region of concern. This suggests that we need further experience and research to evaluate pleural adhesions.

We acquired additional CT images in the affected-side-up lateral position and, therefore, could not avoid additional radiation exposure for the patients. The total estimated radiation exposure for acquiring these additional CT images was acceptable. Moreover, the additional images obtained in the affected-side-up lateral position provided useful information on the relationship between the chest wall and subpleural lung lesions, which was essential for our second-step analysis. The advantage of acquiring these additional images is more meaningful than the disadvantage because of the additional exposure.

In conclusion, our two-step method is a novel, useful, simple, and cost-effective method for evaluating the relationship between the parietal pleura and peripheral pulmonary lesions, especially for excluding the parietal pleural involvement of peripheral pulmonary lesions. Even in cases where respiratory movement is limited—as seen in patients with lesions in the medial and dorsal regions of the upper lobe or in the superior segment of the lower lobe—evaluation of change in position in the second-step analysis is useful for observing the separation between the chest wall and subpleural lung lesions in order to exclude parietal pleural involvement. We believe that this two-step method is practical for use by most CT machines in the world and is, therefore, universally available.

Acknowledgements

We thank our respiratory physicians, Dr. Tetsumoto S, Dr. Tsuruta N, Dr. Niki T, Dr. Toyota S, and Dr. Okamori H for their assistance with clinical management.

References

[1] S.J. UyBico, C.C. Wu, R.D. Suh, N.H. Le, K. Brown, M.S. Krishnam, Lung cancer staging essentials: the new TNM staging system and potential imaging pitfalls, Radiographics 30 (2010) 1163–1181.
[2] F. Facciolo, G. Cardillo, M. Lopergolo, G. Pallone, F. Sera, M. Martelli, Chest wall invasion in non-small cell lung carcinoma: a rationale for en bloc resection, J. Thorac. Cardiovasc. Surg. 121 (2001) 649–656.
[3] H.M. Burkhart, M.S. Allen, F.C. Nichols III, C. Deschamps, D.L. Miller, V.F. Trastek, P.C. Pairolero, Results of en bloc resection for bronchogenic carcinoma with chest wall invasion, J. Thorac. Cardiovasc. Surg. 123 (2002) 670–675.
[4] V.W. Rusch, K.R. Parekh, L. Leon, E. Venkatraman, M.S. Bains, R.J. Downey, P. Boland, M. Bilsky, R.J. Ginsberg, Factors determining outcome after surgical resection of T3 and T4 lung cancers of the superior sulcus, J. Thorac. Cardiovasc. Surg. 119 (2000) 1147–1153.
[5] K. Kawaguchi, S. Mori, N. Usami, T. Fukui, T. Mitsudomi, K. Yokoi, Preoperative evaluation of the depth of chest wall invasion and the extent of combined resections in lung cancer patients, Lung Cancer 64 (2009) 41–44.
[6] P. Uhrmeister, K.H. Allmann, H. Wertzel, C. Altehoefer, J. Laubenberger, J. Hasse, M. Langer, Chest wall infiltration by lung cancer: value of thin-sectional CT with different reconstruction algorithms, Eur. Radiol. 9 (1999) 1304–1309.
[7] T. Higashino, Y. Ohno, D. Takenaka, H. Watanabe, M. Nogami, C. Ohbayashi, M. Yoshimura, M. Satouchi, Y. Nishimura, M. Fujii, K. Sugimura, Thin-section multiplanar reformats from multidetector-row CT data: utility for assessment of regional tumor extent in non-small cell lung cancer, Eur. J. Radiol. 56 (2005) 48–55.
[8] N. Suzuki, T. Saitoh, S. Kitamura, Tumor invasion of the chest wall in lung cancer: diagnosis with US, Radiology 187 (1993) 39–42.
[9] S. Sakai, S. Murayama, J. Murakami, N. Hashiguchi, K. Masuda, Bronchogenic carcinoma invasion of the chest wall: evaluation with dynamic cine MRI during breathing, J. Comput. Assist. Tomogr. 21 (1997) 595–600.
[10] K. Yokoi, K. Mori, N. Miyazawa, Y. Saito, A. Okuyama, M. Sasagawa, Tumor invasion of the chest wall and mediastinum in lung cancer: evaluation with pneumothorax CT, Radiology 181 (1991) 147–152.
[11] K. Ebara, S. Takashima, B. Jiang, H. Numasaki, M. Fujino, Y. Tomita, K. Nakanishi, M. Higashiyama, Pleural invasion by peripheral lung cancer: prediction with three-dimensional CT, Acad. Radiol. 22 (2015) 310–319.
[12] K. Imai, Y. Minamiya, K. Ishiyama, M. Hashimoto, H. Saito, S. Motoyama, Y. Sato, J. Ogawa, Use of CT to evaluate pleural invasion in non-small cell lung cancer: measurement of the ratio of the interface between tumor and neighboring structures to maximum tumor diameter, Radiology 267 (2013) 619–626.
[13] H.S. Glazer, J. Duncan-Meyer, D.J. Aronberg, J.F. Moran, R.G. Levitt, S.S. Sagel, Pleural and chest wall invasion in bronchogenic carcinoma: CT evaluation, Radiology 157 (1985) 191–194.
[14] K. Kuriyama, R. Tateishi, T. Kumatani, K. Kodama, O. Doi, N. Hosomi, Y. Sawai, E. Inoue, T. Kadota, Y. Narumi, Pleural invasion by peripheral bronchogenic carcinoma: assessment with three-dimensional helical CT, Radiology 191 (1994) 365–369.
[15] J.S. Hsu, T.S. Jaw, C.J. Yang, S.F. Lin, M.P. Shih, S.H. Chou, I.W. Chong, M.Y. Lin, I.C. Chiang, Convex border of peripheral non-small cell lung cancer on CT images as a potential indicator of pleural invasion, Medicine (Baltimore) 96 (2017) e7323.
[16] K. Sakuma, T. Yamashiro, H. Moriya, S. Murayama, H. Ito, Parietal pleural invasion/adhesion of subpleural lung cancer: quantitative 4-dimensional CT analysis using dynamic-ventilatory scanning, Eur. J. Radiol. 87 (2017) 36–44.
[17] C.K. Choong, S.S. Pasricha, X. Li, P. Briggs, S. Ramdave, M. Crossett, J.M. Troupis, Dynamic four-dimensional computed tomography for preoperative assessment of lung cancer invasion into adjacent structures, Eur. J. Cardiothorac. Surg. 47 (2015) 239–243.
[18] P.D. Deak, Y. Smal, W.A. Kalender, Multisection CT protocols: sex- and age-specific conversion factors used to determine effective dose from dose-length product, Radiology 257 (2010) 158–166.
[19] S. Sato, Y. Nagatani, M. Hahimoto, N. Nitta, J. Hanaoka, M. Yoshigoe, Y. Oshio, S. Tsukagoshi, H. Otani, K. Murata, Pleural movement against chest wall in pulmonary apical region and its association with ventilation at supine/lateral position assessed by 4D-ULDCT, The 76th Annual Meeting of the Japan Radiological Society ABSTRACTS, JRS (2017) s218.
[20] J. Milic-Emili, J.A. Henderson, M.B. Dolovich, D. Trop, K. Kaneko, Regional distribution of inspired gas in the lung, J. Appl. Physiol. 21 (1966) 749–759.